FULL PAPER

Lubrication Systems

ADVANCED
THEORY AND
SIMULATIONS

www.advtheorysimul.com

Tribo-Induced Structural Transformation and Lubricant Dissociation at Amorphous Carbon–Alpha Olefin Interface

Xiaowei Li,* Aiying Wang, and Kwang-Ryeol Lee*

Amorphous carbon (a-C) combined with a fluid lubricant is capable of providing an ultra-low friction state and thus achieving long lifetime and reliable operation. However, the understanding of the atomistic process occurring at the sliding friction interfaces, especially the interfacial structure transformation and lubricant dissociation at different contact states, is still not well understood. Here, using reactive molecular dynamics simulation, the friction behavior of a self-mated a-C system composited with different alpha olefins (AOs) as lubricants is comparatively investigated, and the results present that due to the co-existence of tribo-induced thermal and shearing effects, AOs exhibit different physicochemical behaviors at the a-C–a-C interface compared to that at the a-C surface. Although introducing AOs into a self-mated a-C system reduces the friction coefficient, its efficiency strongly relies on the AO variety and contact pressure. The pressure-driven dissociation of AOs passivates the friction interface, resulting in the evolution of the primary friction mechanism from hydrodynamic lubrication to interfacial passivation that is not accessible by experimental characterization. The corresponding scission sites of different AOs are demonstrated, which enriches the fundamental understanding on sliding friction behavior and offers a comprehensive design criterion for lubricants (viscosity, chain length, and bond saturated states) and a-C to achieve nearly frictionless sliding interface.

1. Introduction

The development of advanced lubricating system has been unremittingly pursued by modern society to overcome the challenges of energy efficiency and durability caused by friction and wear. A combination of solid lubrication films and fluid lubricants (base oil with additives) can lubricate the moving mechanical components, such as automotive engines and cutting tools,

Dr. X. Li, Dr. K.-R. Lee
Computational Science Center
Korea Institute of Science and Technology
Seoul 136–791, Republic of Korea
E-mail: lixw0826@gmail.com; krlee@kist.re.kr
Dr. X. Li, Dr. A. Wang
Key Laboratory of Marine Materials and Related Technologies
Zhejiang Key Laboratory of Marine Materials and Protective Technologies
Ningbo Institute of Materials Technology and Engineering
Chinese Academy of Sciences
Ningbo 315201, P. R. China

The ORCID identification number(s) for the author(s) of this article can be found under https://doi.org/10.1002/adts.201800157

for easy shearing slippage of contact interfaces, and thus enhance their working life and reliability.[1] As a solid lubrication film, amorphous carbon (a-C) films can sufficiently protect key components against serious mechanical damage due to their high hardness and low friction coefficient.[2–5] Specifically, the self-consumption issue of a-C films, which is accompanied inevitably during the friction process, can be effectively suppressed by compositing with the fluid lubricants,[6,7] and the friction reduction property can be also further improved.[8–11]

The classical Stribeck curve theory[12,13] states that the contact state between the a-C and fluid lubricants can be transformed from the boundary to mixed and hydrodynamic lubrication by tailoring the lubricant variety or critical friction parameters (sliding velocity and contact pressure). Previous studies[14,15] reported that the efficacy of fluid lubricants was commonly governed by the base oil, and Kržan et al.[7] also revealed that the base oil was sufficient for the friction reduction performance of a-C-coated surface. However, commercially available oils are commonly designed for the ferrous surface rather than the a-C surface, and most previous efforts mainly focused on the anti-friction improvement of inorganic and organic additives[16–19] incorporated into fluid lubricants. The interaction between the a-C and base oil at the sliding interface and its dependence on base oil variety are still not well understood, and the underlying friction mechanism in synergism is also not clear due to the complexity of structural evolution of friction interface in experiment.

On the other hand, the friction property is also highly dependent on the contact pressure between the two sliding counterfaces.[3,20,21] Different contact pressures are generated with different contact asperities of a-C surface. Especially, the high contact pressure could be possible for instantaneous contact of a-C asperities during friction process,[22] which may result in the significant dissociation of base oil and interfacial structure transformation significantly.[23] Furthermore, previous reports have adopted molecular dynamics (MD) and first-principles MD methods to study the friction behavior at various contact pressures, such as 4,[24] 5,[25] 10,[23] 19.3,[23] 50,[26,27] and 80 GPa.[24] However, in base oil-lubricated a-C system, the systematical investigation on the structural evolution and corresponding

**ADVANCED
SCIENCE NEWS**

www.advancedsciencenews.com

**ADVANCED
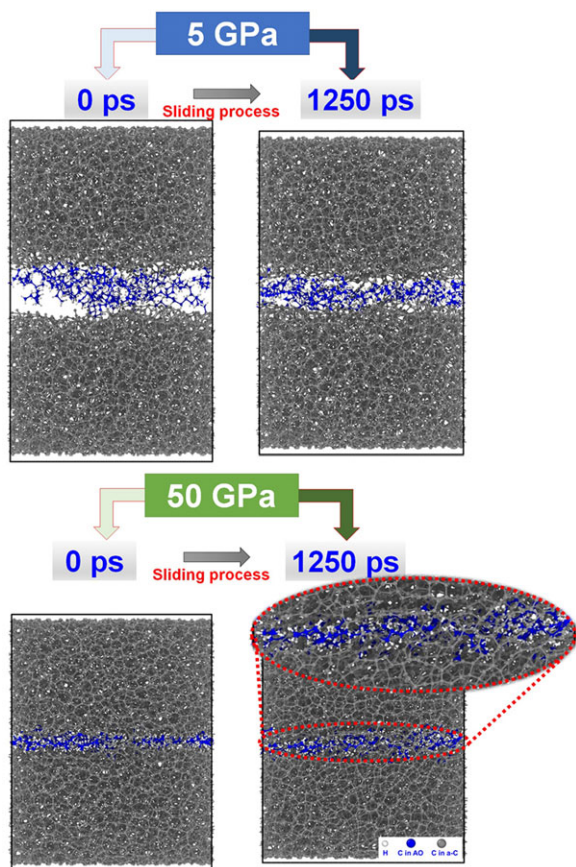THEORY AND
SIMULATIONS**

www.advtheorysimul.com

Figure 1. Morphologies of a-C–C_8H_{16}–a-C friction system before and after the sliding process at different contact pressures.

friction response, which are induced by normal and extreme contact pressures, is also required, which is indispensable for the reliable application of lubricating system in harsh deep-sea or space environment.

In this article, by reactive MD (RMD) simulation using ReaxFF potential,[28,29] we selected different linear alpha olefin (AO) molecules as base oil lubricants and comparatively evaluated the effect of different AOs on the friction behavior of a-C films at different contact pressures. The physicochemical interactions between the a-C and AO molecules and the structural evolution of sliding interface were systematically discussed, which depended closely on the AOs and contact pressures. This study sheds light on the intrinsic mechanism ruling atomic-scale sliding friction that are not accessible by experimental characterization and is expected to provide meaningful insights for designing the novel lubricating systems with high efficiency.

2. Results and Discussion

2.1. Morphologies and Friction Results

Figure 1 shows the morphologies of a-C–C_8H_{16}–a-C friction system before and after the sliding process, while those for C_5H_{10}[30] and $C_{12}H_{24}$ lubricants can be found in Figure S1, Supporting In-

formation. Note that at the same contact pressure, there is no significant difference in the morphologies when the lubricant changes from C_5H_{10} to C_8H_{16} and $C_{12}H_{24}$, while there is a strong dependence on the contact pressure. At the contact pressure of 5 GPa, the AO molecules are uniformly distributed at the interface after the sliding process and two a-C–AO interfaces can be clearly distinguished.[30] With an increase of contact pressure to 50 GPa, compared to the cases before the sliding process, the mixing and interaction between the a-C and AOs enhance drastically after the sliding process, and some AO molecules even bond with C atoms located at the deeper position of a-C structures, suggesting the existence of lubricant dissociation and significant reconstruction of sliding interface,[30] as will be discussed later. This leads to dense but highly distorted structures and the disappearance of sharp a-C–AO interfaces.

Using the friction force and load curves with the sliding time (Figure S2, Supporting Information), the data during the last 200 ps of friction process are adopted to quantify the average friction force and load (**Figure 2**). For comparison, the results in the pure a-C–a-C system without lubricants are also considered. First, it can be noted that compared to the pure case, the addition of AO lubricants reduces the friction force and load simultaneously, but different reduction degrees with contact pressure are observed, and the different loads originate from the change of real contact area at the friction interface. When the contact pressure is 5 GPa (Figure 2a), the average friction force and load with the lubricant from C_5H_{10} to C_8H_{16} and $C_{12}H_{24}$ decrease first and then increase; the friction coefficient gives the similar behavior to the friction force and the minimum friction coefficient of 0.21 is obtained in the a-C–C_8H_{16}–a-C system, which reduces by 97% compared to the pure a-C–a-C case. However, the friction coefficient values are still much larger than those in experiment,[10] attributing to the strong adhesive strength between the two contact surfaces without any passivation or contamination in experiment, but they are still comparable to the previous simulation result.[24,27]

As the system works at a high contact pressure of 50 GPa (Figure 2b), both the average friction force and load drop gradually with lubricants from C_5H_{10} to C_8H_{16} and $C_{12}H_{24}$, being consistent with that of friction coefficient. Although the a-C–$C_{12}H_{24}$–a-C system produces the lowest friction coefficient (0.38), it only drops by 33% compared to the pure case. Especially, the friction coefficient at 50 GPa shows lower sensitivity to lubricant variety than that at 5 GPa, which is a typical feature for the boundary lubrication state.[12,13] Hence, on the one hand, introducing C_5H_{10}, C_8H_{16}, or $C_{12}H_{24}$ into the a-C–a-C sliding interface decreases the friction coefficient, but it works more effectively at the low contact pressure, which is similar to previous study,[30] and the increase of friction coefficient with contact pressure may be related to the strong friction-induced tribochemical reaction at the interface. On the other hand, the selection of lubricant is essential to optimize the friction property, and a lubricant with high viscosity is suggested for systems working at high contact pressure conditions. However, the results presented in Figure 2 raise several fundamental questions: what is the physicochemical behavior (thermal stability, volatility, and degradation) of different AOs on a-C surface? How is the binding state between the a-C and different AOs at the friction interface? How does the evolution of interface structure and properties with AO variety
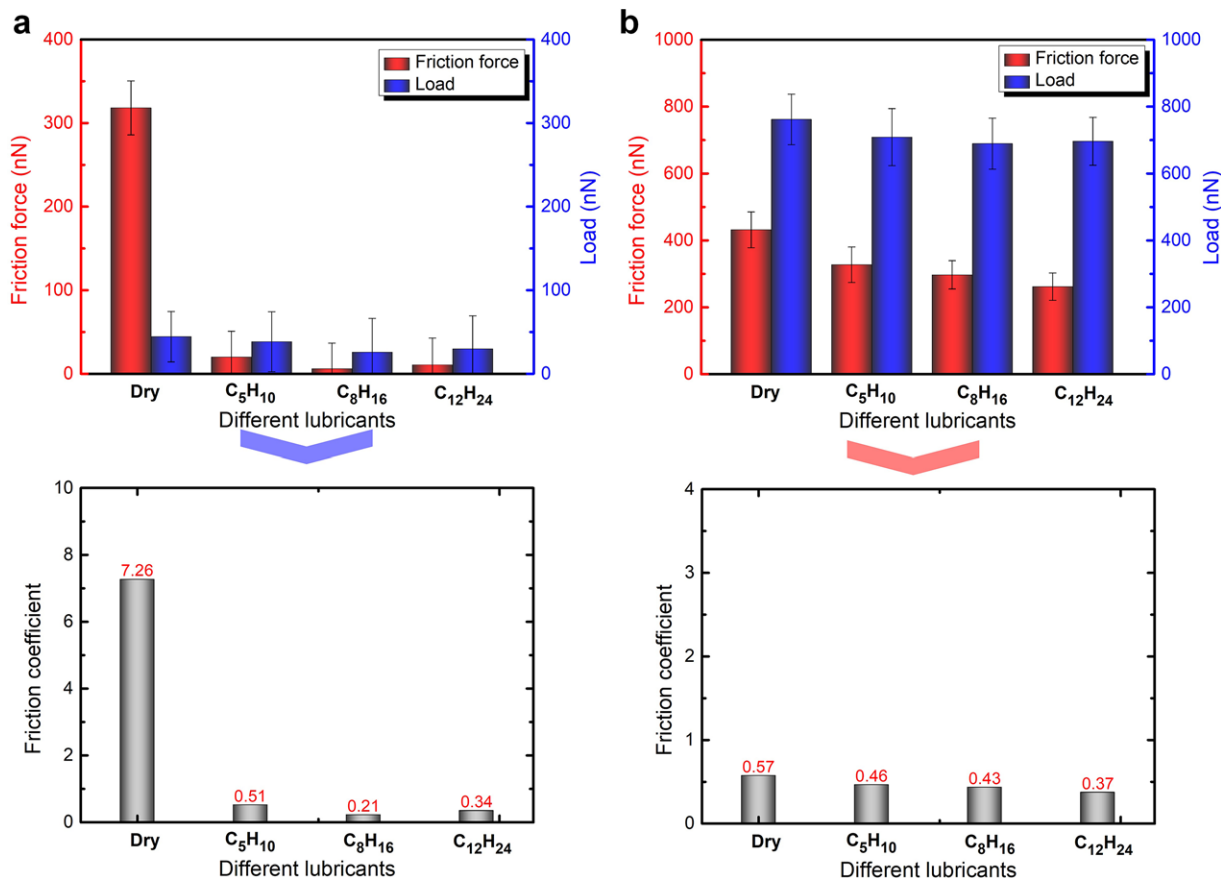
**ADVANCED
SCIENCE NEWS**
www.advancedsciencenews.com

**ADVANCED
THEORY AND
SIMULATIONS**
www.advtheorysimul.com

Figure 2. Friction results including average friction force, average load, and friction coefficient in a-C–AO–a-C systems with different lubricants at contact pressures of a) 5 and b) 50 GPa, respectively. Those for the pure a-C–a-C system without lubricant and with C_5H_{10}[30] are also presented for comparison.

under different contact pressures? Most importantly, what is the underlying lubrication mechanism in the present system: interface passivation, hydrodynamic lubrication, or synergistic effect?

2.2. Intrinsic Physicochemical Behavior of AOs on a-C Surface

In order to answer the first question, the interaction of AOs (C_5H_{10}, C_8H_{16}, and $C_{12}H_{24}$) with a-C structure at different temperatures (300 ≈ 1200 K) is investigated, and the computational details can be found in S1, Supporting Information. **Figure 3**a gives the fraction of remaining intact AO lubricants over temperature for each case. In the a-C-free cases, the AO molecules form cluster configurations at room temperature for each case (see Figure S5, Supporting Information). However, when C_5H_{10}, C_8H_{16}, or $C_{12}H_{24}$ lubricants are introduced onto the a-C surface (Figure S6, Supporting Information), all molecules spread on the surface uniformly at 300 K and there is no evaporation occurring in each case. Nevertheless, after the relaxation at 600 K for 100 ps, the fraction of intact C_5H_{10} molecules decreases to 43% significantly (Figure 3a), while the fractions of remaining intact molecules are 91% for C_8H_{16} and 100% for $C_{12}H_{24}$, respectively. With further increasing the temperature to 900 and 1200 K subsequently, the drastic reduction in fraction of intact molecules is observed

for each case. This originates from not only the evaporation but also the structural degradation of AOs induced by thermal effect.

To explore the thermal degradation of C_5H_{10}, C_8H_{16}, and $C_{12}H_{24}$ lubricants in the presence of a-C structure, the average coordination number of C2, C3, C4, and H atoms in lubricant molecules, which is only contributed by the lubricants, is calculated, as shown in Figure 3b–d. At room temperature, the average coordination number of each atom in lubricant is constant for each case, implying that the lubricants are adsorbed onto the a-C by the intermolecular interaction (see Figure S7, Supporting Information). During relaxation at 600 K for 100 ps, the average coordination numbers of C3 and C4 atoms in C_5H_{10} lubricant (Figure 3b) reduce obviously, indicating the structural degradation mainly occurring at the sites of —CH_2—CH_2— and —CH=CH_2, and the decomposed carbon atoms bond with the a-C structure to passivate the surface (see Figure S7, Supporting Information), but there is almost no degradation observed for C_8H_{16} (Figure 3c) and $C_{12}H_{24}$ (Figure 3d) lubricants. When the temperature further reaches to 900 and 1200 K, severe decomposition is generated for each lubricant by the scissions of all carbon–carbon backbone sites. Hence, compared to the a-C-free cases, the existence of a-C could interact with AO lubricants to inhibit them from escaping the a-C surface and also suppresses the degradation of lubricants at the elevated temperature.
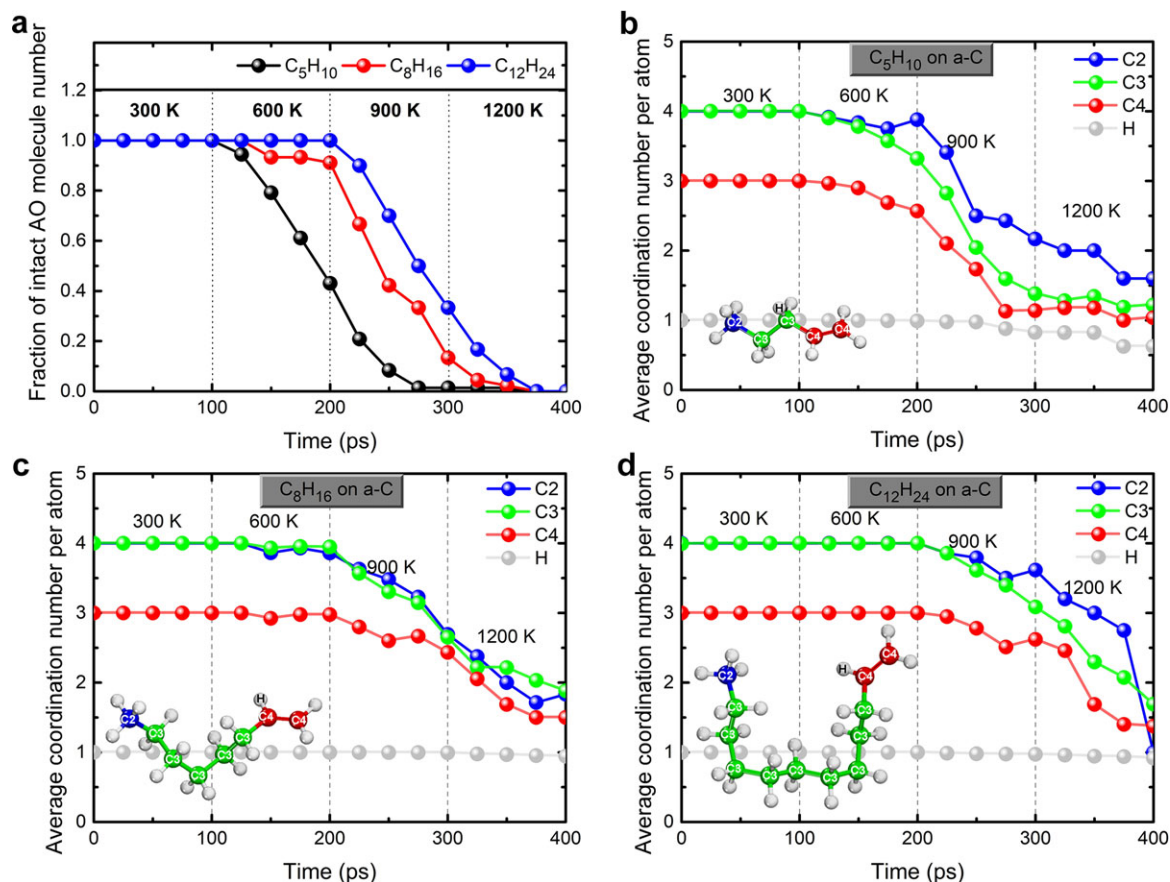
**ADVANCED
SCIENCE NEWS**
www.advancedsciencenews.com

**ADVANCED
THEORY AND
SIMULATIONS**
www.advtheorysimul.com

Figure 3. a) Fraction of remaining intact C_5H_{10}, C_8H_{16}, and $C_{12}H_{24}$ molecules over temperature on a-C surface. Average coordination number of C2, C3, C4, and H atoms in b) C_5H_{10}, c) C_8H_{16}, and d) $C_{12}H_{24}$ lubricant structures as a function of temperature. The contribution of a-C structure to the coordination of lubricant is neglected.

Furthermore, $C_{12}H_{24}$ shows the lowest volatility and the best thermal stability on the a-C surface than C_5H_{10} and C_8H_{16}, but when the temperature is higher than 900 K, there is no AO structure existing stably on the a-C surface for each case, indicating the potential applied environment for these AO lubricants.

2.3. Tribo-Induced Interaction between the a-C and AOs at Friction Interface

During the friction process, the interaction of a-C with AOs is affected by the tribo-induced thermal and shearing effects simultaneously.[3] To answer the second question, the contribution of AO lubricants to the coordination number of the a-C structure is evaluated after the sliding process. For each a-C–AO–a-C friction system at 5 GPa, the AO molecules are distributed at the center of friction interface with a stable plateau region (Figure 1 and Figure S1, Supporting Information) and make no contribution to the coordination of the a-C structure (Figure S8a, Supporting Information), implying the intermolecular interactions between the a-C and AOs. The morphologies with neglected AOs (Figure S8b, Supporting Information) also confirm that the bottom and upper a-C structures are almost completely separated by

the AO lubricants without any direct interaction.[30] In addition, the number of intact AO molecules has no change in any case due to the low shearing stress and flash temperature at the friction-free layer (about 303 ± 1 K) (see Figure S9, Supporting Information). This is consistent with the results in Figure 3. Therefore, the interfacial structure contributed by a-C and AOs can be evaluated independently, and the friction behavior at such low contact pressure may be attributed to the hydrodynamic lubrication caused by C_5H_{10}, C_8H_{16}, or $C_{12}H_{24}$ lubricants.[12,13,30,31]

Figure 4 shows the coordination number distribution of the a-C structure at a contact pressure of 50 GPa, which results from the AO contribution and the morphologies after sliding process. The morphologies distinctly exhibit the severe interfilm interactions between the bottom and upper a-C structures, suggesting the boundary lubrication state.[12,13,30] The C3 and C4 atoms in AOs contribute to the coordination of a-C structures, indicating the presence of tribochemical interactions including bond breaking and re-bonding of AOs with a-C.[23] Especially, with the lubricant evolving from C_5H_{10} to C_8H_{16} and $C_{12}H_{24}$, the contribution of C4 atoms to the coordination number of a-C decreases, while the C3 contribution increases, different from the thermal effect shown in Figure S7, Supporting Information. This behavior is related to the number of C3 and C4 atoms in the system, but most importantly, it provides a clue to
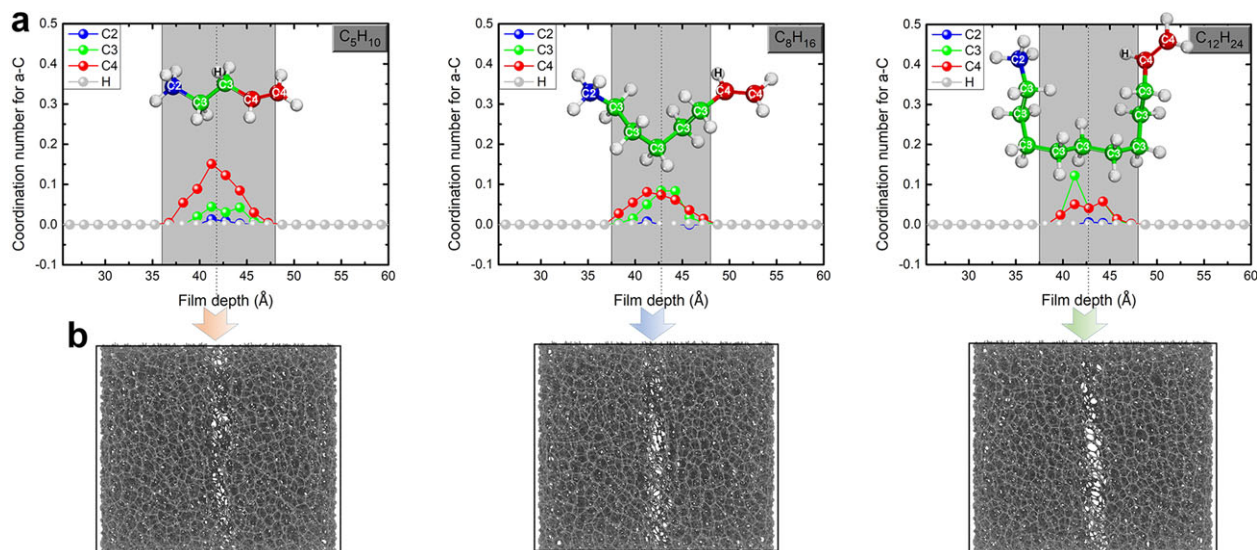
**ADVANCED
SCIENCE NEWS**

www.advancedsciencenews.com

**ADVANCED
THEORY AND
SIMULATIONS**

www.advtheorysimul.com

Figure 4. a) Coordination number distribution of C atoms in the a-C structure, which is contributed by AO lubricants only, and b) morphologies of the friction systems (lubricants are neglected for view) after sliding process at the contact pressure of 50 Gpa, in which the results for C_5H_{10} are also given for comparison. Reproduced under the terms of the CC BY 4.0 license.[30] Copyright 2018, The Authors, Published by Springer Nature.
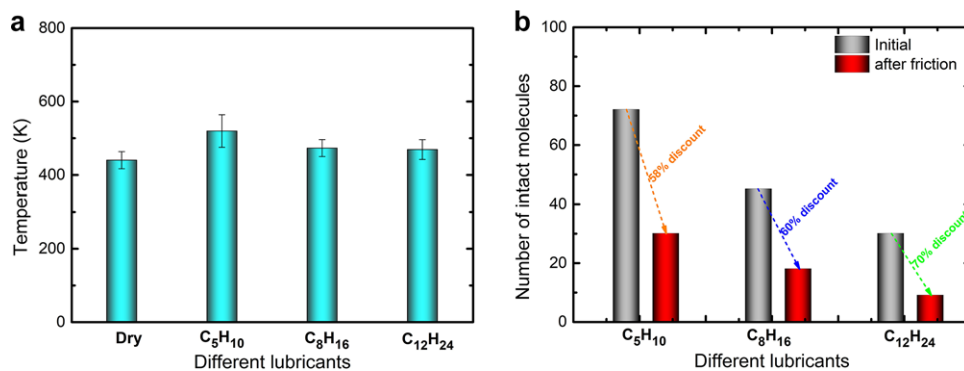

Figure 5. a) Average temperature of the free layer during the steady-state friction stage as a function of AO lubricants when the contact pressure is 50 GPa. b) Number of intact C_5H_{10}, C_8H_{16}, or $C_{12}H_{24}$ molecules in a-C–AO–a-C friction system after sliding process at the contact pressure of 50 GPa.

achieve the functionalized a-C surface by modifying the specific bonding site of lubricants, such as $-CH=CH_2$ site for C_5H_{10} and $-CH_2\euro\euro\euro CH_2-$ site for $C_{12}H_{24}$. In addition, although the high friction forces (Figure 2b) result in the increase of flash temperatures at the sliding interface (**Figure 5**a), the number of intact C_5H_{10}, C_8H_{16}, or $C_{12}H_{24}$ molecules significantly decreases by 58%, 60%, or 70%, respectively (Figure 5b), which is much higher than those in Figure 3a. In particular, note that $C_{12}H_{24}$ displays the most serious dissociation than the other two AO lubricants, which is contrary to the intrinsic nature of AOs on a-C surface, as illustrated in Figure 3. This indicates that the structural stability of AO at the a-C–a-C friction interface is mainly dominated by the shearing effect, which is different from the catalyst-induced dissociation of AO reported by Erdemir,[1] and an AO lubricant with long chain length is easier to be broken on a rough a-C surface due to the tribo-induced shearing effect.

Furthermore, **Figure 6** displays the AO structure and bonding ratios between the C2, C3, and C4 atoms of AO lubricants for each system at 50 GPa. The bonding ratio, B_{ab}, is evaluated as follows:[30]

$$B_{ab} = \frac{N_{ab}^t}{N_{ab}^0} \tag{1}$$

where, N_{ab}^0 and N_{ab}^t are the total bond numbers of atom a with atom b when the sliding time is 0 or t ps; a and b range from atom C2 to C3 and C4, respectively, in AO molecules. Owing to the dissociation of AO lubricants, there are many fragments at the interface for each case. Notably, Figure 6a shows that for C_5H_{10},[30] the bonding ratios of B_{33} for C3—C3 bonds and B_{44} for C4—C4 bonds significantly decrease by 57% and 37%, respectively, following decreases of 10% in B_{23} and 14% in B_{34}. Thus, the scission of their carbon–carbon backbones mainly occurs at the $-CH=CH_2$ and $-CH_2-CH_2-$sites, which is consistent with that induced by thermal effect (Figure 3b). However, for C_8H_{16}, the bonding ratios in Figure 6b confirm that the structural dissociation is mainly achieved through the scission of the $-CH=CH_2$ and $-CH_2-CH=$sites with 38% and 31% reduction in the bonding numbers, respectively, while the dissociation of the $C_{12}H_{24}$ lubricant mainly originates from the scission
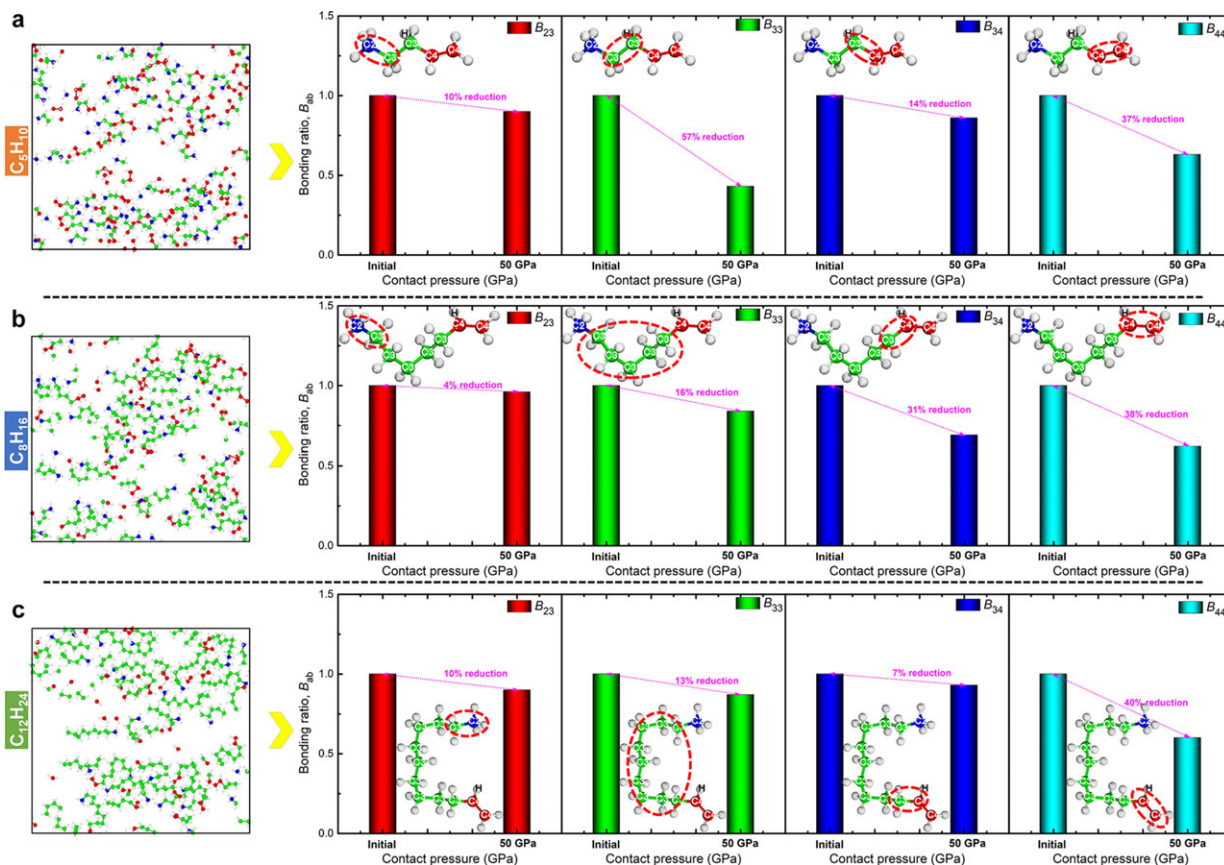
**ADVANCED
SCIENCE NEWS**

www.advancedsciencenews.com

**ADVANCED
THEORY AND
SIMULATIONS**

www.advtheorysimul.com

Figure 6. Lubricant structure and bonding ratios between the C2, C3, and C4 atoms of lubricants in the system with a) C_5H_{10}, b) C_8H_{16}, and c) $C_{12}H_{24}$ as lubricants, respectively, after sliding process at the contact pressure of 50 GPa. a) Reproduced under the terms of the CC BY 4.0 license.[30] Copyright 2018, The Authors, Published by Springer Nature.

of −CH=CH_2 with 40% reduction (Figure 6c). Additionally, for each case, the double bonds mainly contribute to the dissociation of the lubricants, which are unfavorable for the structural stability of the lubricant.[30] However, their dissociation could also passivate the dangling bonds of friction interface.

Therefore, the high contact pressure produces the high shearing stress and interfacial temperature, which lead to the drastic dissociation of the lubricant[30] and the reconstruction of interfacial structure.[30,32] The dissociated AOs re-bond and mix with a-C to form the dense and distorted interface with enhanced passivation of dangling bonds, dominating the friction property of the system but also weakening the hydrodynamic lubrication. Besides, there is no dehydrogenation observed for each case (Figure S10, Supporting Information), unlike in a previous study where the Cu substrate catalyzed the serious breaking of C−H bonds in AO lubricant.[1]

2.4. Evolution of Structural Property of Interfacial with AOs

It is well known that the friction property is strongly correlated with the structural properties of the interface, which is required to clarify the underlying friction mechanism. Before characterizing the structural properties of interface, the distributions of density, residual stress, and coordination number along the z di-

rection are analyzed first to define the width of the interfacial region, as shown in **Figure 7**. For each case, the system is divided into three regions, including the bottom intrinsic a-C, interface, and upper intrinsic a-C regions.[30] In the system at 5 GPa (Figure 7a), when the lubricant changes from C_5H_{10} to C_8H_{16} and $C_{12}H_{24}$, the widths of the interfacial regions are 18.0 (blue background), 19.5 (red background), and 19.5 Å (green background), respectively, while they decrease to 12 (blue background), 10.5 (red background), and 10.5 Å (green background), respectively, at 50 GPa (Figure 7b). Using these values, the properties (density and residual stress) of the friction interface are quantified.

Figure 8 shows the variations of density and residual stress of interface with AOs, which are contributed by a-C and AO lubricants separately. Compared to the dry conditions, introducing AO into the a-C–a-C system leads to the reduction of interfacial density, but the density values from a-C or AO contributions slightly depend on AO variety. However, the obvious evolution of residual stress as a function of lubricants is observed. At 5 GPa (Figure 8a), the residual stress evolves from the tensile state for the dry condition to the compressive state for the AO condition. This implies a higher sp^3 fraction at the interface according to the P–T diagram,[27,30,33] in which a high compressive stress favors the formation of the sp^3 structure. In addition, with the lubricants changed from C_5H_{10} to C_8H_{16} and $C_{12}H_{24}$, the contribution of a-C to the compressive stress first decreases and then increases,

ADVANCED
SCIENCE NEWS
www.advancedsciencenews.com

ADVANCED
THEORY AND
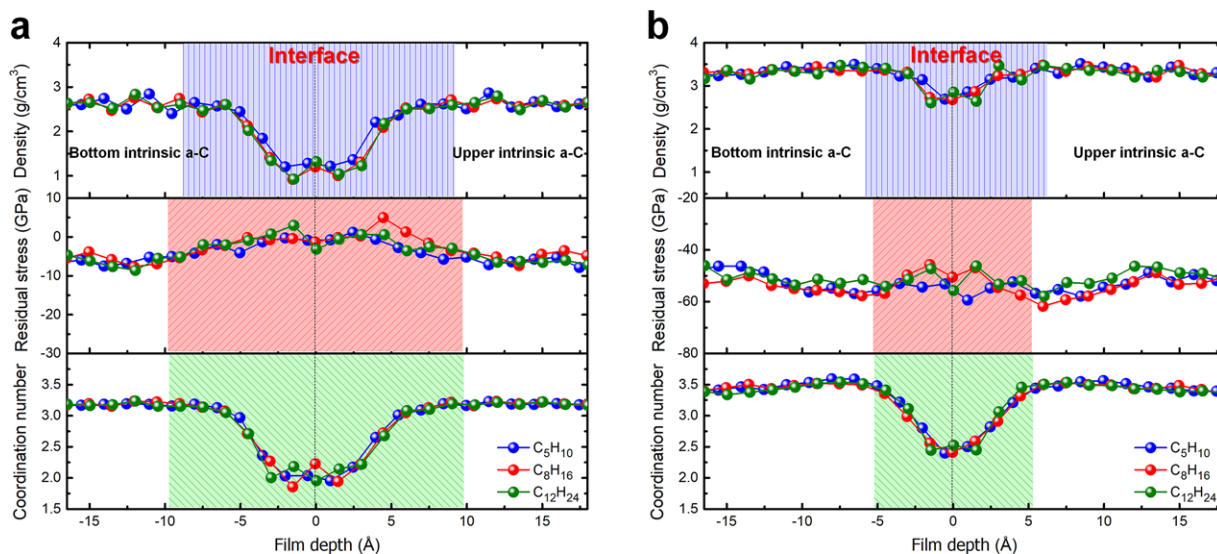**SIMULATIONS**
www.advtheorysimul.com

Figure 7. Distributions of density, residual stress, and coordination number along the *z* direction in a-C–AO–a-C systems with different AO lubricants and under contact pressures of a) 5 and b) 50 GPa, respectively, in which blue, red, and green colors represent the width of interfacial region as the lubricants range from C_5H_{10} to C_8H_{16} and $C_{12}H_{24}$.
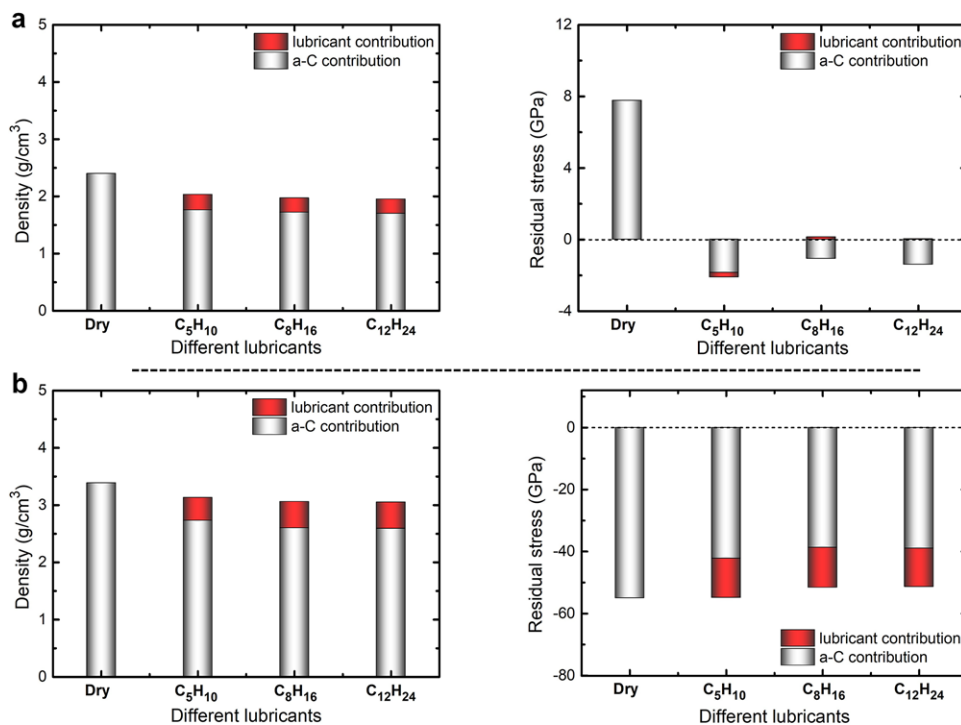

Figure 8. Density and residual stress of the interface contributed by a-C and AO lubricants separately in the system after sliding process at contact pressures of a) 5 GPa and b) 50 GPa, respectively. The results of the pure a-C–a-C system without lubricant are also evaluated for comparison.

which is related to the complicated interactions between the bottom and upper a-C surfaces or the a-C and AOs. A further increase of contact pressure to 50 GPa (Figure 8b) promotes the dissociation of AO lubricants and the reconstruction of interfacial structure,[30,33] leading to the compressive stress value for each case, which is close to that under dry condition. Therefore, the density and residual stress of the interface at high contact pressure are little dependent on the AO variety.

Combined with the interfacial density and residual stress (Figure 8), the hybridization structure of the interface and mean square displacement (MSD) of C_5H_{10}, C_8H_{16}, or $C_{12}H_{24}$ lubricants provide insights into understanding the mechanism in synergism (Q4). In the system at 5 GPa, the AOs are adsorbed onto the a-C surface by intermolecular interactions rather than chemical bonding; therefore, the hybridization structure of a-C and the mobility of AOs are evaluated separately, as shown in
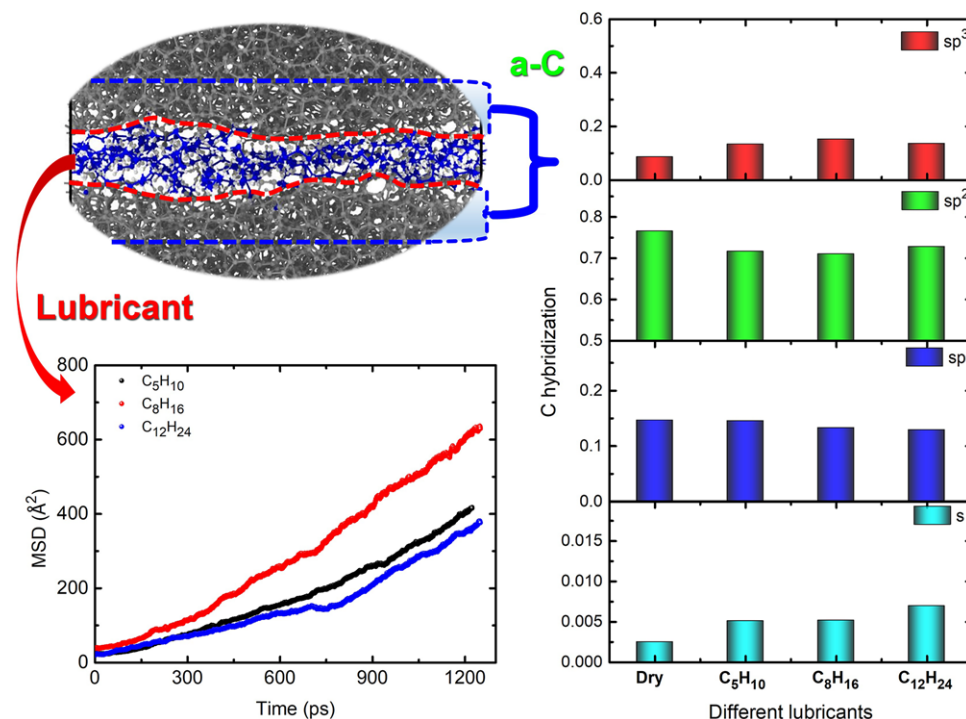
**ADVANCED
SCIENCE NEWS**

www.advancedsciencenews.com

**ADVANCED
THEORY AND
SIMULATIONS**

www.advtheorysimul.com

Figure 9. Hybridization structure of a-C at the interface and MSD of C_5H_{10}, C_8H_{16}, or $C_{12}H_{24}$ lubricants in the a-C–AO–a-C friction system at the contact pressure of 5 GPa. The results of the pure a-C–a-C system without lubricant are also evaluated for comparison.

Figure 9. First, compared to the interfacial structure before loading (sp² fraction, 62.9 at.%), the increased sp² fraction is observed for each case, suggesting the presence of sp³-to-sp² transformation, which coincides with the observation in the experiment.[10] However, compared to the case under dry condition when C_5H_{10} is used as lubricant,[30] the transformation of residual stress from tensile to compressive state (Figure 8a) induced the decrease in both the un-passivated sp and sp² fractions of the a-C surface after the sliding process following the increase in sp³ fraction (Figure 9),[3,27,30,33] suggesting the passivation of a-C sliding surface. On the other hand, owing to the weak intermolecular interactions between the a-C and C_5H_{10}, MSD result shows that the C_5H_{10} lubricant can migrate easily, indicating that the hydrodynamic lubrication from C_5H_{10} determines the friction behavior and thus accounts for the significant reduction of friction coefficient (Figure 2a). When the lubricant is C_8H_{16} instead of C_5H_{10}, the mobility of C_8H_{16} lubricant is further improved, and the sp² and sp fractions are also further reduced, resulting in the lowest friction coefficient. However, in the a-C–$C_{12}H_{24}$–a-C system, the sp² and sp fractions increase and the mobility of $C_{12}H_{24}$ lubricant on the rough a-C surface is also restrained due to the increased chain length, inducing the increased friction coefficient (Figure 2a).

When the contact pressure is 50 GPa, the strong tribochemical interaction between the a-C and AOs and the dissociation of AOs occur for all systems with different AOs (Figure 6), the dissociated fragments from the lubricants can passivate the a-C surface (Figure 4), and thus the friction behavior is mainly affected by the reconstructed interface consisting of a-C and lubricants.[30,32] **Figure 10** shows the carbon hybridization structure of the whole interface composed of a-C and AO lubricant. Compared to the

case at dry sliding, although the reduction of compressive stress in the a-C–C_5H_{10}–a-C system (Figure 8b) induces the increase of un-passivated sp² and sp fractions through the sp³-to-sp² and sp³-to-sp transformations, the large amount of intact C_5H_{10} molecules, remaining after the friction process, still dominates the decrease of friction coefficient (Figure 2b).[30] When the lubricant is C_8H_{16} instead of C_5H_{10}, the un-passivated C–C bonds (sp² and sp) continue to increase, but the friction coefficient almost has no change (from 0.46 for C_5H_{10} to 0.43 for C_8H_{16}) because of the slightly improved mobility of C_8H_{16} lubricant. However, when the $C_{12}H_{24}$ lubricant is introduced into the a-C–a-C friction interface, the drastic dissociation of $C_{12}H_{24}$ molecules (Figure 5b) weakens the mobility of the lubricant (Figure 10), but it can be compensated by further passivating the interfacial structure, which is achieved by the re-bonding between the $C_{12}H_{24}$ fragments and the sp- and sp²-C atoms of a-C surface (Figure 4) and thus accounts for the slight drop in the friction coefficient.

3. Conclusion

We performed RMD simulations using the ReaxFF force field to comparatively investigate the effect of different AO lubricants on the friction behavior of a-C–a-C system under different contact conditions. By systematically analyzing the interaction of AO with a-C, the tribo-induced dissociation of AOs, the structure and property of interface, the MSD of AO lubricants, and the friction coefficient, results suggested the following

- Friction property was closely dependent on the AO variety and the contact state between the a-C and AOs.
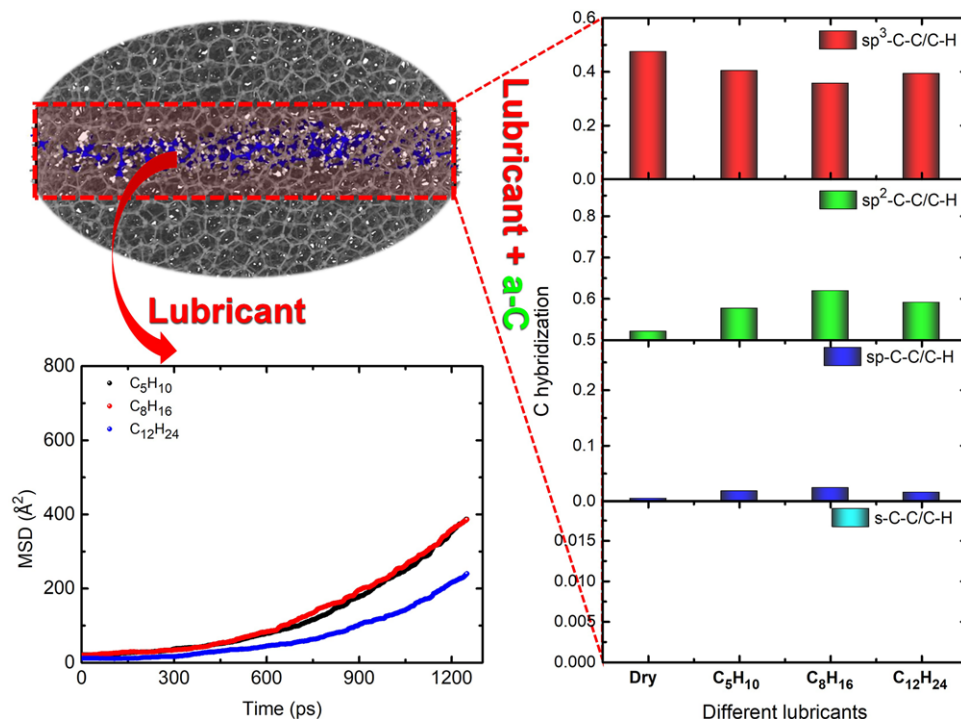
**ADVANCED
SCIENCE NEWS**
www.advancedsciencenews.com

**ADVANCED
THEORY AND
SIMULATIONS**
www.advtheorysimul.com

Figure 10. Hybridization structure of interface including a-C and lubricant and MSD of C_5H_{10}, C_8H_{16}, or $C_{12}H_{24}$ lubricants in the a-C–AO–a-C friction system at the contact pressure of 50 GPa. The results of the pure a-C–a-C system without lubricant are also evaluated for comparison.

- Compared to the intrinsic nature of lubricants on a-C surface, due to the existence of both the tribo-induced thermal and shearing effects, AOs at the friction interface exhibited different behaviors of structural stability, dissociation, and passivation to the a-C structure.

- At the low contact pressure of 5 GPa, a-C interacted with the lubricant via intermolecular interactions; the dependence of friction coefficient on AO variety was mainly attributed to the difference in hydrodynamic lubrication of AOs, although the interfacial passivation also contributed to the friction behavior; the a-C–C_8H_{16}–a-C exhibited the lowest friction coefficient, which reduced by 97% compared to the case under dry sliding condition.

- When the contact pressure increased to 50 GPa, it not only induced the tribochemical interaction between the a-C and the AO lubricants, but also inspired the structural transformation of interface from sp^3-C to sp^2-C and sp-C. The synergism in thermal and shearing effect resulted in the drastic dissociation of AO molecules at different sites of the carbon–carbon backbones, and the AO lubricant with long chain length was easier to be broken on a rough a-C surface, which was contrary to the intrinsic nature of AO molecules. In particular, with AOs ranging from C_5H_{10} to C_8H_{16} or $C_{12}H_{24}$, the C atoms in —CH_2€€€CH_2—site of AO mainly contributed to the interfacial passivation instead of CH_2=CH—site. The structural passivation of friction interface, combined with the hydrodynamic lubrication of AOs, could account for the evolution of friction coefficient with AOs.

- The results span the range between organic chemistry, surface science, and engineering application, and guide both the scientific understanding and technical implementation of the a-

C–AO system for tribo-application. Considering the structural diversity of a-C films, future improvements will focus on the dependence of friction behavior on the a-C structure in a-C–AO systems.

4. Experimental Section

Fabrication of Friction Model and Related Parameters: All RMD calculations were performed using the large-scale atomic/molecular massively parallel simulator (LAMMPS).[34] Figure S11, Supporting Information, shows the "sandwich" model of a-C–AO–a-C friction system, which consisted of lower a-C substrate, middle AO lubricant, and upper a-C counterface. The a-C structure with a size of 42.88 × 40.358 × 31 Å^3 was fabricated by the atom-by-atom deposition method[35] and composed of 6877 carbon atoms. The linear AOs with different chain lengths including C_5H_{10}, C_8H_{16}, and $C_{12}H_{24}$ were selected as lubricants, in which the results in C_5H_{10}-lubricated system were referred from our previous study[30] for comparison, and the corresponding viscosities at 300 K were 0.19, 0.44, and 1.19 mPa·s, respectively. The AO molecule numbers were 72 for C_5H_{10}, 45 for C_8H_{16}, and 30 for $C_{12}H_{24}$ separately in order to treat the mass as constant. The bottom layer of a-C substrate and the top layer of a-C counterface within a thickness range of 5 Å were held firm. Moving toward the interface, the structures in the next thickness of 5 Å of both the substrate and counterface were coupled to 300 K using the microcanonical ensemble with Berendsen thermostat.[36] Other remaining atoms from the a-C and AOs were completely unconstrained to move during the friction process. The time step was 0.25 fs and the periodic boundary condition was set along the *x* and *y* directions.

Friction Simulation Process: During the friction simulation, the geometry optimization for the whole system was first implemented at 300 K for 2.5 ps, and then the upper a-C counterface was loaded toward the lubricants and bottom a-C substrate until a specified value of contact pressure was achieved during 25 ps. Next, the rigid layer of upper a-C counterface

was given a constant sliding velocity (10 m s^{-1}) along the x direction for 1250 ps to reach the steady-state friction state. After the friction process, the friction force and load values acting on the fixed atoms of the lower a-C substrate were adopted to calculate the friction coefficient. During the short MD simulation time, in order to achieve different contact states at the sliding interface, a normal contact pressure of 5 GPa and extreme contact pressure of 50 GPa were considered, respectively, according to the reports by Li,[30] Zilibotti,[23] and Ma.[24] Although these values were much higher than that in experiment, previous studies[22–27,30] had clearly confirmed that it was appropriate and necessary for examining the friction behavior on an atomic scale. In addition, it should be mentioned that the load values, generated at the same contact pressure, were different from previous reports.[24,25,37] This was attributed to the difference in the surface state (hybridization, adatom passivation, and roughness) of a-C structure, suggesting that the direct and accurate comparison between macro- and microscopic results remains a big challenge until now.

ReaxFF Potential Validation: The ReaxFF potential[28,29] was used to describe the interactions between the carbon and hydrogen atoms, and the reliability of the method was validated to be suitable for carbon-based structures. However, additional calculations including the formation energy of C_5H_{10} under different temperatures and the adsorption energy of C_5H_{10} on a-C surface with different densities were also undertaken by RMD and ab-initio calculations[38,39] separately. Figure S12, Supporting Information, clearly discloses that the RMD results agreed well with those from ab-initio calculations. In addition, the a-C structures were fabricated by quenching method (see S3, Supporting Information), and the corresponding results also displayed that the sp^3 fraction–density relationship from RMD calculation was well reproduced compared to previous calculation[40] and experimental result.[41] Furthermore, the ReaxFF potential was adopted to simulate the growth of a-C films using the atom-by-atom deposition approach, and the results were as illustrated in S4, Supporting Information, indicating that ReaxFF[29] accurately described the structural properties of a-C films through comparison with the widely accepted AIREBO potential.[42] Hence, the above-mentioned calculations confirmed the validity of the ReaxFF[29] potential for the simulated system.

Supporting Information

Supporting Information is available from the Wiley Online Library or from the author.

Conflict of Interest

The authors declare no conflict of interest.

[1] A. Erdemir, G. Ramirez, O. L. Eryilmaz, B. Narayanan, Y. Liao, G. Kamath, S. K. R. S. Sankaranarayanan, *Nature* **2016**, *536*, 67.
[2] J. Robertson, *Mater. Sci. Eng., R* **2002**, *37*, 129.
[3] L. Cui, Z. Lu, L. Wang, *Carbon* **2014**, *66*, 259.
[4] J. Vetter, *Surf. Coat. Technol.* **2014**, *257*, 213.
[5] J. Huang, L. Wang, B. Liu, S. Wan, Q. Xue, *ACS Appl. Mater. Interfaces* **2015**, *7*, 2772.
[6] J. M. Martin, M. I. D. B. Bouchet, C. Matta, Q. Zhang, W. A. Goddard III, S. Okuda, T. Sagawa, *J. Phys. Chem. C* **2010**, *114*, 5003.
[7] B. Kržan, F. Novotny-Farkas, J. Vižintin, *Tribol. Int.* **2009**, *42*, 229.
[8] M. Kano, *Tribol. Int.* **2006**, *39*, 1682.
[9] J. Ye, Y. Okamoto, Y. Yasuda, *Tribol. Lett.* **2008**, *29*, 53.
[10] H. A. Tasdemir, M. Wakayama, T. Tokoroyama, H. Kousaka, N. Umehara, Y. Mabuchi, T. Higuchi, *Tribol. Int.* **2013**, *65*, 286.
[11] K. K. Mistry, A. Morina, A. Neville, *Wear* **2011**, *271*, 1739.
[12] E. R. M. Gelinck, D. J. Schipper, *Tribol. Int.* **2000**, *33*, 175.
[13] B. J. Hamrock, S. R. Schmid, B. O. Jacobson, *Fundamentals of Fluid Film Lubrication*, 2nd ed., Marcel Dekker, New York **2005**.
[14] R. I. Taylor, R. C. Coy, *P. I. Mech. Eng.* **2000**, *214*, 1.
[15] S. C. Tung, M. L. McMillan, *Tribol. Int.* **2004**, *37*, 517.
[16] J. Qu, W. C. Barnhill, H. Luo, H. M. Meyer III, D. N. Leonard, A. K. Landauer, B. Kheireddin, H. Gao, B. L. Papke, S. Dai, *Adv. Mater.* **2015**, *27*, 4767.
[17] L. Austin, T. Liskiewicz, I. Kolev, H. Zhao, A. Neville, *Surf. Interface Anal.* **2015**, *47*, 755.
[18] H. Okubo, C. Tadokoro, S. Sasaki, *Wear* **2015**, *332–333*, 1293.
[19] X. Fan, L. Wang, *Sci. Rep.* **2015**, *5*, 1.
[20] D. W. Kim, K. W. Kim, *Wear* **2013**, *297*, 722.
[21] J. Sun, Y. Zhang, Z. Lu, Q. Li, Q. Xue, S. Du, J. Pu, L. Wang, *J. Phys. Chem. Lett.* **2018**, *9*, 2554.
[22] Y. Mo, K. T. Turner, I. Szlufarska, *Nature* **2009**, *457*, 1116.
[23] G. Zilibotti, S. Corni, M. C. Righi, *Phys. Rev. Lett.* **2013**, *111*, 146101.
[24] T. B. Ma, L. F. Wang, Y. Z. Hu, X. Li, H. Wang, *Sci. Rep.* **2015**, *4*, 3662.
[25] S. Bai, H. Murabayashi, Y. Kobayashi, Y. Higuchi, N. Ozawa, K. Adachi, J. M. Martin, M. Kubo, *RSC Adv.* **2014**, *4*, 33739.
[26] Y. N. Chen, T. B. Ma, Z. Chen, Y. Z. Hu, H. Wang, *J. Phys. Chem. C* **2015**, *119*, 16148.
[27] T. B. Ma, Y. Z. Hu, H. Wang, *Carbon* **2009**, *47*, 1953.
[28] S. G. Srinivasan, A. C. T. Van Duin, P. Ganesh, *J. Phys. Chem. A* **2015**, *119*, 571.
[29] F. Tavazza, T. P. Senftle, C. Zou, C. A. Becker, A. C. T. Van Duin, *J. Phys. Chem. C* **2015**, *119*, 13580.
[30] X. Li, A. Wang, K. R. Lee, *npj Comput. Mater.* **2018**, *4*, 53.
[31] M. Kalin, I. Velkavrh, *Wear* **2013**, *297*, 911.
[32] T. Kuwahara, G. Moras, M. Moseler, *Phys. Rev. Lett.* **2017**, *119*, 096101.
[33] D. R. McKenzie, D. Muller, B. A. Pailthorpe, *Phys. Rev. Lett.* **1991**, *67*, 773.
[34] S. Plimpton, *J. Comput. Phys.* **1995**, *117*, 1.
[35] X. Li, P. Ke, H. Zheng, A. Wang, *Appl. Surf. Sci.* **2013**, *273*, 670.
[36] H. J. C. Berendsen, J. P. M. Postma, W. F. van Gunsteren, A. DiNola, J. R. Haak, *J. Chem. Phys.* **1984**, *81*, 3684.
[37] H. Lan, T. Kato, C. Liu, *Tribol. Int.* **2011**, *44*, 1329.
[38] G. Kresse, J. Furthmüller, *Comput. Mater. Sci.* **1996**, *6*, 15.
[39] G. Kresse, J. Furthmüller, *Phys. Rev. B* **1996**, *54*, 11169.
[40] K. J. Koivusaari, T. T. Rantala, S. Leppävuori, *Diamond Relat. Mater.* **2000**, *9*, 736.
[41] P. J. Fallon, V. S. Veerasamy, C. A. Davis, J. Robertson, G. A. J. Amaratunga, W. I. Milne, J. Koskinen, *Phys. Rev. B* **1993**, *48*, 4777.
[42] S. J. Stuart, A. B. Tutein, J. A. Harrison, *J. Chem. Phys.* **2000**, *112*, 6472.